Article

Journal of
Nanoscience and Nanotechnology
Vol. 15, 9002–9008, 2015
www.aspbs.com/jnn



# Improved Sensing Behaviors in Reduced Graphene Oxide Functionalized with $Ni(OH)_2$ Nanoparticles

Han Gil Na[1], Yong Jung Kwon[1], Hong Yeon Cho[1], Sung Yong Kang[1], Taek Kyun Jung[2,3], Hyo-Soo Lee[2], and Hyoun Woo Kim[1,*]

[1]*Division of Materials Science and Engineering, Hanyang University, Seoul 133-791, Republic of Korea*
[2]*Rare Metals R&D Group, Korea Institute of Industrial Technology, 7-47 Songdo-dong, Yeonsu-gu, Incheon 406-840, Republic of Korea*
[3]*Department of Materials Science and Engineering, Inha University, Incheon 402-751, Republic of Korea*

In this paper, we detail improvements in the sensing properties of reduced graphene oxide (RGO), which were achieved through functionalization. The functionalization process utilizes graphene oxide suspensions, generating nanoparticles on the RGO surface mainly comprised of $Ni(OH)_2$ phase. Raman spectra indicate that functionalization increases the degree of disorder in RGOs. $NO_2$ gas sensing tests reveal an approximate increase of 154% in the sensor response of the RGOs after functionalization. Possible mechanisms for improving sensing responses via functionalization are discussed. The enhancement is due to the spillover effect, to the increase of the sensor surface by the catalytic particles, to the reduction of RGO conduction volume through the generation of depletion region, and to the resistance modulation of the heterojunctions.



**Keywords:** Nanoparticles, Reduced Graphene Oxide, Sensors.

## 1. INTRODUCTION

A variety of nanostructures has attracted enormous attention, as a result of their novel properties.[1–16] A variety of graphene and graphene oxide structures have promising sensing characteristics.[17–21] In particular, pure graphene has been investigated as a sensor candidate for various gases, including $NO_2$,[22] $NH_3$,[23] $CO_2$,[24] $O_2$,[25] and $H_2$.[26] reduced graphene oxides (RGOs) have several advantages as gas sensors in comparison to pure graphene. RGO is cheaper and more easily available than pure graphene, and requires a simpler fabrication procedure where graphene oxide is heated which enables large-scale production.[27] RGO also possesses a superior adsorption probability which is critical for detection of gas because the surface is modified or functionalized. In spite of its many advantages, the sensing behavior of RGO has yet to be fully investigated.

Numerous studies have investigated the catalytic effects of metal nanoparticles on sensing behavior. Pt nanoparticles in particular are effective in not only enhancing the gas sensing behavior of RGO with respect to $O_2$,[28] glucose,[29] hydrogen peroxide,[30] and hydrogen,[31] but also enhancing electrochemical sensing capability.[32]

Various Ni nanoparticles, including Ni, $Ni(OH)_2$, and NiO, have been investigated for their catalytic roles in sensing. Ni-nanoparticle-decorated titania nanotubes have been used as nonenzymatic glucose sensors.[33] $Ni(OH)_2$ nanoparticles have been added to glassy carbon, not only for selectively sensing dopamine and serotonin in the presence of ascorbic acid,[34] but also for enhanced sensing of 4-chlorophenol.[35] $Ni(OH)_2$ nanoparticles have been used as humidity sensors,[36] and NiO hollow microspheres have been applied in gas sensors.[37] NiO nanoparticles have been used as sensing electrodes in $NO_2$ sensors,[38] and NiO nanoparticles were immobilized onto a DNA-modified electrode to prepare a highly-sensitive, enzymeless glucose sensor.[39]

In this work, we have prepared the first $Ni(ON)_2$ nanoparticle decorated RGO. We have compared functionalized and pristine RGO in regard to structure, morphology, Raman, and gas sensing properties.

## 2. EXPERIMENTAL DETAILS

We have used graphite powder, $H_2SO_4$ (98%), $H_3PO_4$ (98%), $KMnO_4$ (98%), $H_2O_2$ (30 wt%), Hydrazine

*Author to whom correspondence should be addressed.


1533-4880/2015/15/9002/007 doi:10.1166/jnn.2015.11571

monohydrate (98%), DMF (99.8%) and Boric acid ($H_3BO_3$), all obtained from commercial resources, as source materials. Graphene oxide (GO) was synthesized from graphite powder via a modification of Hummers' and Offeman's methods (see Supplementary material).[40]

The experimental procedure for the preparation of RGO-Cu is summarized in Figure 1, with procedural schematics shown in Figure 2. The GO suspension was comprised of GO powders (150 mg) and 10 mmol of deionized (DI) water (500 ml). The mixture of GO powders and DI water was sonicated for 1 h, resulting in a GO suspension. The GO suspension was then mixed with a solution consisting of 25 mmol of $Pt(NH_3)_2(NO_2)_2$ (10 g, Pt 5 wt% solution), 25 mmol of Ni salt (625 mg), 2 M-NaOH (20 ml), and DI water (100 ml). This solution was maintained at 80 °C for 5 h. At this stage, the metal-related particles have been attached to the GO (Fig. 2). It is noteworthy that 2 M-NaOH facilitated the oxidation of Ni-related nanoparticles. First, low-speed centrifugation at 4000 rpm removed thick multilayer sheets (15–20 min). A second, high-speed step at 8000–12000 rpm for 45 min removed the liquid solid solution, producing solid GO-nanoaprticles composites. The high-speed centrifugation was performed several times, finally lowering the pH to 7. The product was then heated to 90 °C using a vacuum dry oven for 5 h. In order to prepare RGO-nanoaprticle composites, an annealing reaction was performed at 400 °C for 5 h in an Ar and $H_2$ environment using a horizontal tube furnace.

The samples were characterized via X-ray diffraction (XRD; *D/MAX Rint 2000* diffractometer model, Rigaku, Tokyo, Japan, CuK$\alpha$ radiation), field-emission scanning electron microscopy (FESEM, JSM-6700, JEOL Ltd., Tokyo, Japan), and transmission electron microscopy (TEM; JEOL JEM-2010 transmission electron microscope, JEOL Ltd., Tokyo, Japan, 200 kV). Raman spectra were obtained at room temperature, with an excitation laser wavelength and power density of 532 nm and 2.9 $mW \cdot cm^{-2}$, respectively. X-ray photoelectron spectroscopy (XPS) (VG Multilab ESCA 2000 system, UK) was carried out with a monochromatized Al K$\alpha$ X-ray source ($h\nu = 1486.6$ eV) to investigate the elemental compositions. A Jasco Laser Raman Spectrophotometer (NRS-3000 Series at Korean Basic Science Institute (KBSI)) was employed.

$NO_2$ gas was used to investigate gas sensing properties. Ni/Au double-layer electrodes were deposited onto the specimens with an interdigitated electrode mask. The sensor device was placed into a vacuum chamber with a base pressure of $\sim 5 \times 10^{-6}$ Torr, and a measurement temperature of 250 °C. A similar experimental setup was previously reported.[41–44] The sensor response was estimated using the following formula: $S = R_a/R_g$, where $R_a$ and $R_g$ are resistances in ambient air and $NO_2$ gas, respectively. The response and recovery times were defined as the time to reach a 90% change in resistance via the supply or removal, respectively, of the target gas.[45]



## 3. RESULTS AND DISCUSSION

Figures 3(a)–(c) exhibit the XRD patterns of GO, RGO, and functionalized RGO, respectively. In Figure 3(b), a strong and sharp (002) diffraction line from RGO can be

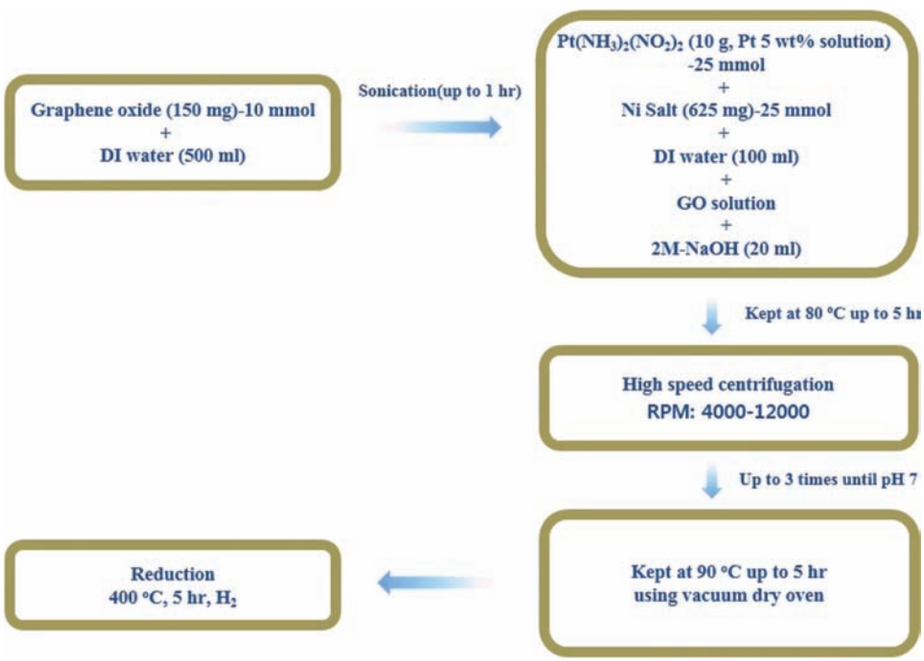


**Figure 1.** Summary of procedures for the fabrication of Cu-functionalized GO and RGO.

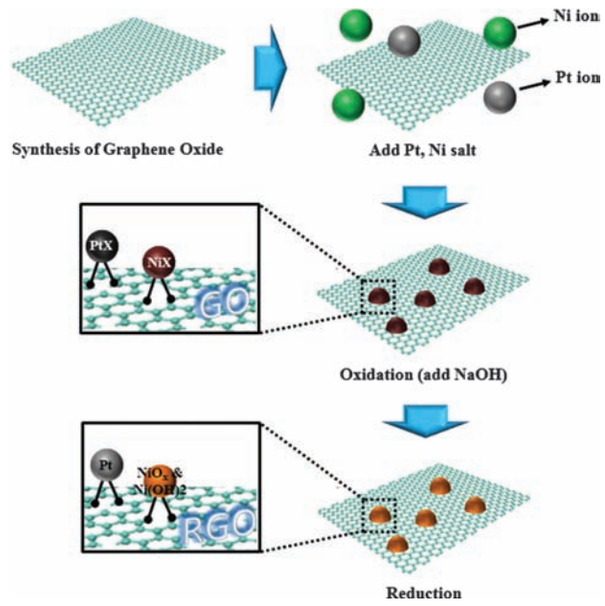


**Figure 2.** Schematic outline of the fabrication of Cu-functionalized GO and RGO.

observed at $2\theta = 25.60°$.[46] Figure 3(c) shows an XRD pattern of the functionalized RGO, with (001), (101), (102), and (111) diffraction lines of the hexagonal nickel hydroxide ($Ni(OH)_2$) phase with lattice constants of $a = 3.126$ Å and $c = 4.605$ Å (JCPDS card: No. 14-0117), and the (200) line of cubic NiO with a lattice constant of $a = 4.1771$ Å (JCPDS card: No. 47-1049). The (220) line of NiO coincides with the (111) line of $Ni(OH)_2$. Additionally, the pattern comprises a diffraction peak of cubic Pt with a lattice constant of $a = 3.9231$ Å (JCPDS card: No. 04-0802).



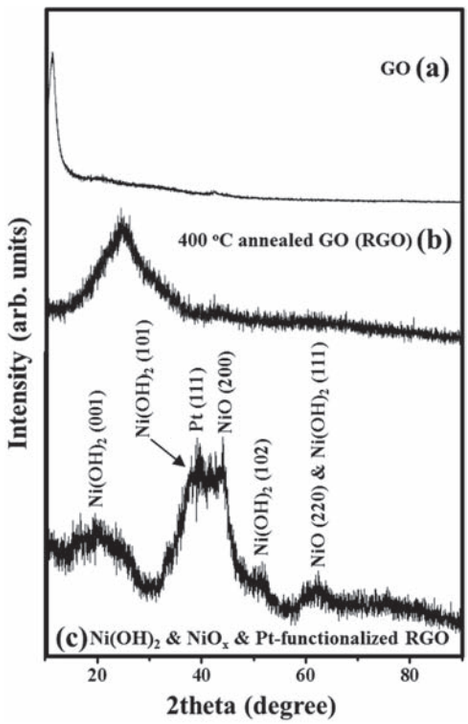


**Figure 3.** XRD spectra of (a) GO, (b) RGO, and (c) functionalized RGO.

Figures 4(a) and (c) show SEM images of as-synthesized and functionalized RGO, respectively, with no apparent differences. Figure 4(d) shows the enlarged image, revealing that the functionalized RGO is comprised of particle-like structures on the surface. Figures 5(a) and (b) show low- and higher-magnification TEM images of the functionalized RGO, respectively, where dark nanoparticles appear on the surface of the RGO.

Figure 5(c) exhibits the lattice-resolved TEM image of the RGO, in which the lattice planes of dark nanoparticles are clearly observed. Through careful examination of the pertinent figures, we conclude that the nanoparticles are single-phased, being comprised of Pt, NiO, and $Ni(OH)_2$. The lattice fringes observed in a nanoparticle in Figure 5(c) correspond to the (200) lattice plane of cubic Pt, with a spacing of 0.196 nm. Another nanoparticle exhibits fringe corresponding to the (111) lattice plane of cubic Pt. The spacing between the lattice planes of a NiO nanoparticle is approximately 0.147 nm, corresponding to the $d_{220}$ spacing of a cubic NiO phase. We reveal that the interplanar spacing of a $Ni(OH)_2$ nanoparticle is approximately 0.233 nm, which corresponds to the (101) plane of hexagonal $Ni(OH)_2$. Figure 5(d) shows the associated SAED pattern with four distinct diffraction rings, corresponding to the (101) plane of $Ni(OH)_2$, (200) plane of NiO, (200) plane of Pt, and (220) plane of NiO, respectively. Accordingly, the SAED pattern reveals that there are numerous nanoparticles with Pt, NiO, and $Ni(OH)_2$ phases.

Figures 6(a)–(c) show the first-order Raman spectra of as-synthesized GO, as-synthesized RGO, and functionalized RGO, respectively. In our preliminary experiments, the precursor graphite exhibited a highly ordered

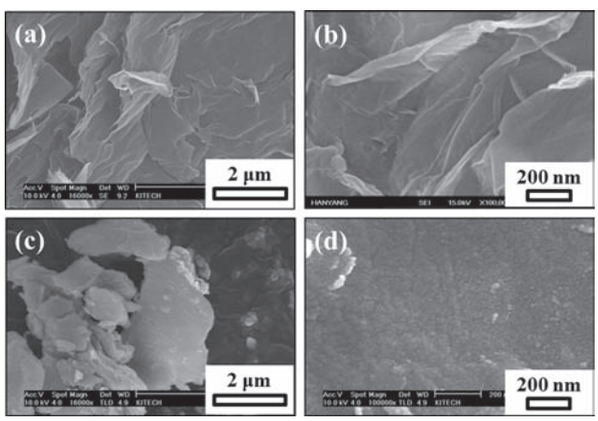


**Figure 4.** (a) SEM images and (b) enlarged images of as-synthesized RGO. (c) SEM images and (d) enlarged images of functionalized RGO.

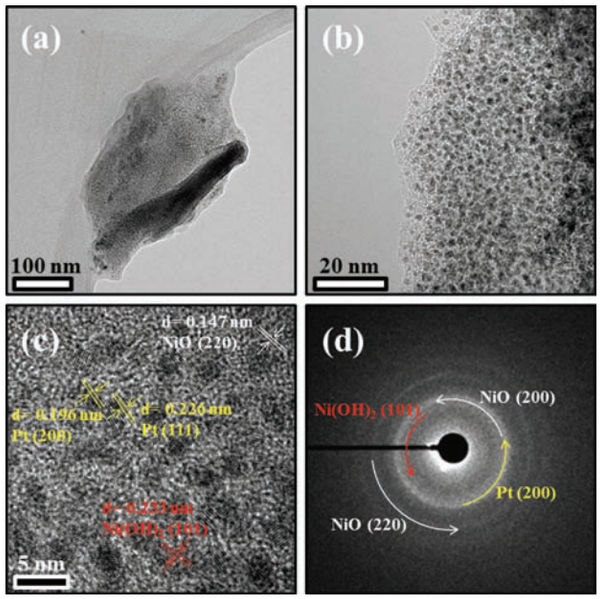


**Figure 5.** (a) Low-magnification TEM image and (b) enlarged TEM image of functionalized RGO. (c) Lattice-resolved TEM image, and (d) associated SAED pattern.

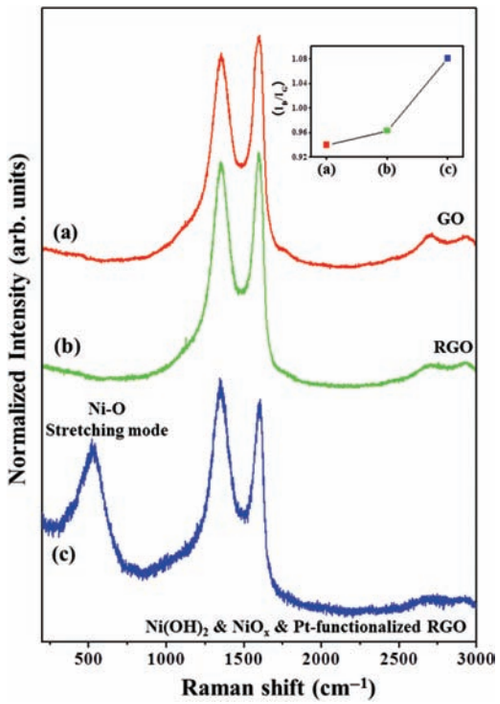


**Figure 6.** First-order Raman spectra of (a) as-synthesized GO, (b) as-synthesized RGO, and (c) functionalized RGO.

nature,[47] with the value of the intensity ratio of the D and G bands ($I_{(D)}/I_{(G)}$) measured at approximately 0.10. The $I_{(D)}/I_{(G)}$ values of as-synthesized GO, as-synthesized RGO, and functionalized RGO measure at 0.94, 0.96, and 1.08, respectively. As the $I_{(D)}/I_{(G)}$ value increases, the disorder in the structure also increases. Accordingly, the increase of the $I_{(D)}/I_{(G)}$ value from 0.94 to 0.96 confirms that the RGO became more disordered than the GO. Similarly, the increase in the $I_{(D)}/I_{(G)}$ value via functionalization indicates that the functionalization process increases the degree of disorder in GO. On the other hand, the G-band frequencies of as-synthesized GO, as-synthesized RGO, and functionalized RGO are 1599.1, 1595.9, and 1604.1 $cm^{-1}$, respectively. With the G band of pristine graphite being located at the lower frequency of 1582 $cm^{-1}$, the increase in G-band-frequency corresponds to the destruction of a conjugated system in the graphite, which is due to oxidation.

XPS measurements were carried out in order to investigate the chemical composition of the products. A raw-scan XPS spectrum of functionalized RGO is shown in Figure 7(a), with several peaks, including O1s, C1s, Ni3p, Pt4f, Ni3s, Ni2s, $Ni2p_{1/2}$, $Ni2p_{3//2}$, Ni LMM, NiLMM1, and NiLMM2, revealing the existence of C, O, Pt, and Ni elements. Figures 7(b)–(d) show the high-resolution scan spectra of $Pt_{4f}$, $Ni_{2p2/3}$, and $O_{1s}$, respectively. Curve fitting was performed using a Gaussian-Lorentzian peak shape after performing a Shirley background correction. Figure 7(b) shows the 4f7/2 and 4f5/2 doublets of Pt(0), Pt(II), and Pt(IV), which are typical peaks for Pt nanostructures. The XPS spectra of the $Ni_{2p2/3}$ states are shown in Figure 7(c), where a main peak can be observed near ~856 eV, presumably corresponding to the combination of the $Ni^{2+}(2p_{3/2})$ and $Ni^{3+}(2p_{3/2})$ electronic states of the Ni, in addition to the electron-loss peak above 860 eV. It is known that the $Ni^{3+}$ ionic state is not an energetically favorable charge compensating state in the case of NiO.[48,49] It is noteworthy that there is no peak near ~852 eV, which is associated with the nickel ($Ni^0$) state;[50] accordingly, we surmise that there is no pure Ni phase in the product.

By analyzing Figures 7(a) and (d), we estimate that the percentage of Pt, NiO, and $Ni(OH)_2$ phases are 8.2, 6.0, and 85.8%, respectively. Accordingly, it is reasonable to assume that the sensor response is mainly enhanced by $Ni(OH)_2$ catalyst.

Figures 8(a) and (b) show the dynamic response curves at a $NO_2$ concentration of 100 ppm for the sensors fabricated from as-synthesized and functionalized RGO, respectively. It is noteworthy that the resistance was decreased and increased upon introducing and removing the $NO_2$ gas, respectively. The RGO sensors correspond to *p*-type whether or not the functionalization has been carried out. From the measured resistance values and the formula $S = R_a/R_g$, where $R_a$ and $R_g$ are resistances in ambient air and $NO_2$ gas, respectively, respectively, we have calculated the sensor responses of the sensors. The sensor responses of as-synthesized and functionalized RGO are calculated at approximately 1.01 and 2.57, respectively, indicating that the sensor response to $NO_2$

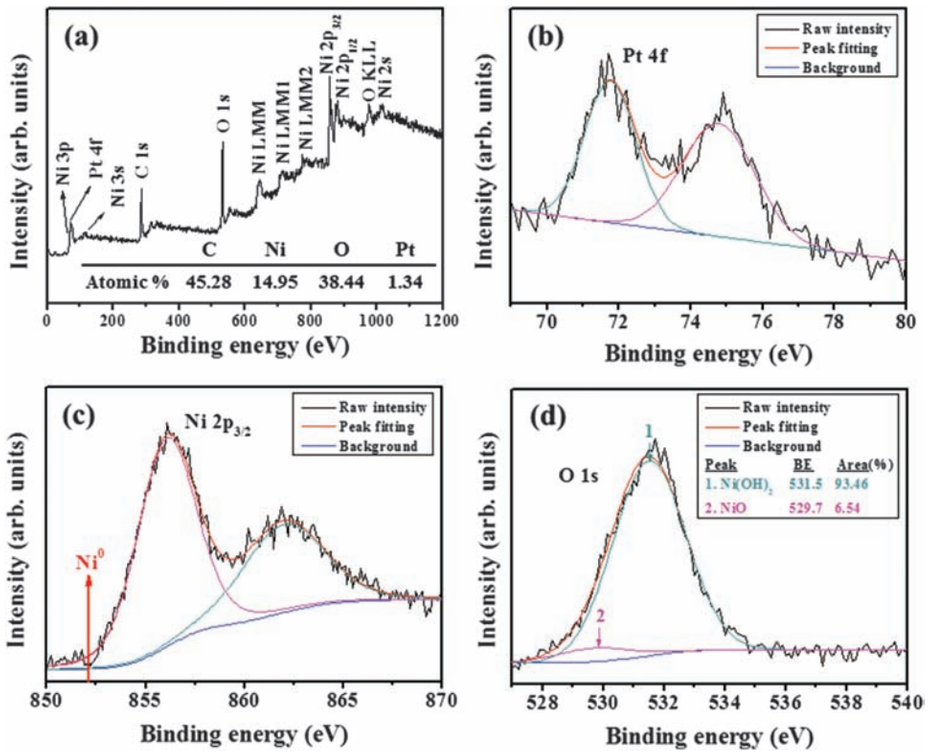


**Figure 7.** (a) Raw-scan XPS spectra of functionalized RGO. (b) High-resolution XPS spectra for (b) $Pt_{4f}$, (c) $Ni_{2p2/3}$, and (d) $O_{1s}$.



gas was drastically enhanced via functionalization. The response times of the as-synthesized and functionalized RGO are 929 and 3081 s, respectively, and the recovery times of the as-synthesized and functionalized RGO are 4889 and 6968 s, respectively.

RGO has been shown to possess *p*-type semiconductor characteristics.[51, 52] The $NO_2$ gas extracts electrons from the RGO surface, increasing positive holes in the RGO and thus decreasing the *p*-type resistivity. We discuss the reason for the enhancement of sensitivity by the functionalization. First, by means of the functionalization, the decorated RGO will have a larger surface area, facilitating molecular absorption, gas diffusion, and mass transport.

Second, the nanoparticles will exert a spillover effect, by which the adsorption, dissociation, and reaction of gas molecules are promoted.

Third, the NiO/RGO and $Ni(OH)_2$/RGO interfaces will generate the *p*–*p* heterojunctions. It is generally known that NiO is a *p*-type semiconductor with a bandgap from 3.6 to 4.0 eV,[53–55] whereas the bandgap energy of *p*-type $Ni(OH)_2$ ranges from 3.04 to 3.06 eV.[56] In addition, the Schottky barrier or interface voltage will appear at the Pt/RGO junctions. Since the dominant phase of the nanoparticles is the $Ni(OH)_2$, we suggest that the presence of *p*-$Ni(OH)_2$/*p*-RGO heterojunctions will be responsible for generating depletion regions, decreasing the conduction volume and thus increasing the sensitivity. Also, the heterojunctions will induce the resistance modulation, contributing to the increase of the sensitivity.

Figure 8(c) reveals increases in both response and recovery times via functionalization. Here we have assumed that the $Ni(OH)_2$ sites play dominant catalytic roles in enhancing the sensing behavior. There are two possible reasons for the elongation of response and recovery times via functionalization. First, this phenomenon will be associated with the occurrence of a catalytic particle-RGO potential barrier. The generated charge depletion region beneath the catalytic particles will scatter the holes in RGOs, decreasing the charge mobility.[57] Second, the diameter of catalytic particles is greater than the electron (hole) mean free path, contributing to the increase in response/recovery times. Similarly, Kauffman et al. reported that the response of CNTs to the CO gas grew longer via Au nanoparticle-decoration.[58] We expect that the generation of defective sites on RGO surface will decrease the response time. If the ratio of high-energy to low-energy binding sites increases, the adsorption behavior will be enhanced, leading to reduction of response times. However, it is possible that the recovery times can be increased, by the increase of the ratio of high-energy to low-energy binding sites. The additional surface treatment will be needed to decrease the recovery times. Further detailed study is underway, which will be reported in the following paper.

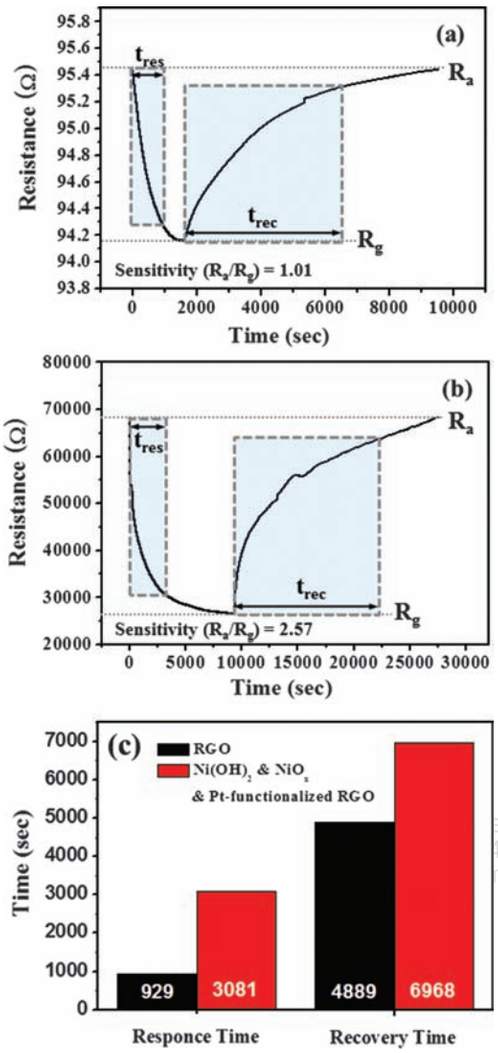


**Figure 8.** Dynamic response curves at $NO_2$ concentration of 100 ppm for sensors fabricated from (a) as-synthesized and (b) functionalized RGO. (c) Graph showing the response and recovery times for sensors fabricated from as-synthesized and functionalized RGO.

## 4. CONCLUSION

In summary, we have fabricated functionalized RGOs, which were obtained from GO suspensions mixed with $Pt(NH_3)_2(NO_2)_2$, Ni salt, NaOH, and DI water. XRD patterns, SAED patterns, and lattice-resolved TEM images of the functionalized-RGO coincidentally reveal the presence of Pt, NiO, and $Ni(OH)_2$ phases. However, quantitative analysis based on XPS revealed that the dominant phase of the nanoparticles corresponded to $Ni(OH)_2$. Raman spectra reveal that the functionalized RGO is more disordered than pristine RGO. The sensor responses of as-synthesized and functionalized RGOs are approximately 1.01 and 2.57, respectively, indicating that functionalization significantly enhances sensor response to $NO_2$ gas. The enhanced sensor response is surmised to result from the spillover effect, in which the $Ni(OH)_2$ sites play a dominant role in the adsorption of $NO_2$ molecules. In addition, the sensitivity will be enhanced, not only by the reduction of RGO conduction volume through the generation of depletion region, but also by the resistance modulation of the heterojunctions. Also, the increase of the sensor surface by the functionalization will contribute to the sensor enhancement. Both response and recovery times were increased via functionalization. We hypothesize that several mechanisms drive this result, including the catalytic particles-RGO potential barrier and the presence of catalytic particles with diameters greater than the charge carrier mean free path. The response/recovery times will be further controlled to meet the requirements of future sensors.

**Acknowledgment:** This work was supported by the National Research Foundation of Korea (NRF) grant funded by the Korea government (MSIP) (No. NRF-2014M2B2A4031881).

## References and Notes

1. A. Sarkar, K. Kanakamedala, N. N. Jagadish, A. Jordan, S, Das, N. Siraj, I. M. Warner, and T. Daniels-Race, *Electron. Mater. Lett.* 10, 879 (**2014**).
2. Y. A. K. Reddy, B. Ajitha, P. S. Reddy, M. S. P. Reddy, and J.-H. Lee, *Electron. Mater. Lett.* 10, 907 (**2014**).
3. S. Kim, G. Nam, and J.-Y. Leem, *Electron. Mater. Lett.* 10, 915 (**2014**).
4. S. B. Jambure, G. S. Gund, D. P. Dubal, S. S. Shinde, and C. D. Lokhande, *Electron. Mater. Lett.* 10, 943 (**2014**).
5. H.-A. Choi, H. Jang, H. Hwang, M. Choi, D. Lim, S. E. Shim, and S.-H. Baeck, *Electron. Mater. Lett.* 10, 957 (**2014**).
6. N. K. Singh, B. Choudhuri, A. Mondal, J. C. Dhar, T. Goswami, S. Saha, and C. Ngangbam, *Electron. Mater. Lett.* 10, 975 (**2014**).
7. J. S. Maeng, D. J. Choi, K.-O. Ahn, and Y.-H. Kim, *Electron. Mater. Lett.* 10, 1019 (**2014**).
8. L. R. Shobin and S. Manivannan, *Electron. Mater. Lett.* 10, 1027 (**2014**).
9. M. Zhuang, A. Wei, J. Liu, Y. Zhao, and Z. Yan, *Electron. Mater. Lett.* 10, 1075 (**2014**).
10. S.-K. Kim, C. J. Raj, and H.-J. Kim, *Electron. Mater. Lett.* 10, 1137 (**2014**).
11. R. Yu, J.-H. Pee, H.-J. Kim, and Y. J. Kim, *Electron. Mater. Lett.* 10, 1159 (**2014**).
12. Y.-S. Cho and Y.-D. Huh, *Electron. Mater. Lett.* 10, 1185 (**2014**).
13. Y. D. Jo, S. Lee, J. Seo, S. Lee, D. Ahn, and H. Lee, *J. Nanosci. Nanotechnol.* 14, 9148 (**2014**).
14. Y. K. Kin, S. Cha, J. H. Lee, and S. H. Hong, *J. Nanosci. Nanotechnol.* 14, 9143 (**2014**).
15. K. S. Min, K. S. Kim, K. N. Kim, A. Mishra, and G. Y. Yeom, *J. Nanosci. Nanotechnol.* 14, 9108 (**2014**).
16. J. H. Son, Y. H. Song, B. J. Kim, and J.-L. Lee, *Electron. Mater. Lett.* 10, 1171 (**2014**).
17. K. S. Novoselov, A. K. Geim, S. V. Morozov, I. V. Grigorieva, and A. A. Firsov, *Science* 306, 666 (**2004**).
18. F. Yavari, Z. Chen, A. V. Thomas, W. Ren, H. M. Cheng, and N. Koratkar, *Sci. Rep.* 1, 166 (**2011**).
19. W. Yuan, A. Liu, L. Huang, C. Li, and G. Shi, *Adv. Mater.* 25, 766 (**2013**).
20. G. H. Lu, S. Park, K. H. Yu, R. S. Ruoff, L. E. Ocola, D. Rosenmann, and J. H. Chen, *ACS Nano* 5, 1154 (**2011**).
21. G. H. Lu, L. E. Ocola, and J. H. Chen, *Appl. Phys. Lett.* 94, 083111 (**2009**).

**22.** W. Yuan, A. Liu, L. Huang, C. Li, and G. Shi, *Adv. Mater.* 25, 766 (**2013**).
**23.** J. D. Fowler, M. J. Allen, V. C. Tung, Y. Yang, R. B. Kaner, and B. H. Weiller, *ACS Nano* 3, 301 (**2009**).
**24.** H. J. Yoon, D. H. Jun, J. H. Yang, Z. Zhou, S. S. Yang, and M. M. C. Cheng, *Sens. Actuators B* 157, 310 (**2011**).
**25.** M. S. Chung, A. Mayer, B. L. Weiss, N. M. Miskovsky, and P. H. Cutler, *Appl. Phys. Lett.* 98, 243502 (**2011**).
**26.** L. S. Zhang, W. D. Wang, X. Q. Liang, W. S. Chu, W. G. Song, W. Wang, and Z. Y. Wu, *Nanoscale* 3, 2458 (**2011**).
**27.** G. Lu, S. Park, K. Yu, R. S. Ruoff, L. E. Ocola, D. Rosenmann, and J. Chen, *ACS Nano* 5, 1154 (**2011**).
**28.** S. S. Kim, J. Y. Park, S.-W. Choi, H. S. Kim, H. G. Na, J. C. Yang, and H. W. Kim, *Nanotechnology* 21, 415502 (**2010**).
**29.** L.-Q. Rong, C. Yan, Q.-Y. Qian, and X.-H. Xia, *Talanta* 72, 819 (**2007**).
**30.** C. Guzman, G. Orozco, Y. Verde, S. Jimenez, L. A. Godinez, E. Juaristi, and E. Bustos, *Electrochim. Acta* 54, 1728 (**2009**).
**31.** D.-T. Phan and G.-S. Chung, *Sens. Actuators B Chem.* 161, 341 (**2012**).
**32.** S. Shahrokhian, N. Hosseini-Nassab, and Z. Kamalzadeh, *J. Sol. Stat. Electrochem.* 18, 77 (**2014**).
**33.** S. J. Yu, X. Peng, G. Z. Cao, M. Zhou, L. Qiao, J. Y. Yao, and H. C. He, *Electrochim. Acta* 76, 512 (**2012**).
**34.** A. Babaei and A. R. Taheri, *Sens. Actuators B Chem.* 176, 543 (**2013**).
**35.** J. Zolgharnein, T. Shariatmanesh, and A. Babaei, *Sens. Actuators B Chem.* 186, 546 (**2013**).
**36.** V. Jeseentharani, M. George, B. Jeyaraj, A. Dayalan, and K. S. Nagaraja, *J. Experiment. Nanosci.* 8, 358 (**2013**).
**37.** G. X. Zhu, C. Y. Xi, H. Xu, D. Zheng, Y. J. Liu, X. Xiang, and X. P. Shen, *RSC Adv.* 2, 4236 (**2012**).
**38.** L. Wang, Z.-C. Hao, L. Dai, Y. H. Li, H. Z. Zhou, *Mater. Lett.* 87, 24 (**2012**).
**39.** E. Sharifi, A. Salimi, E. Shams, A. Noorbakhsh, and M. K. Amini, *Biosens. Bioelectron.* 56, 313 (**2014**).
**40.** W. S. Hummers and R. E. Offeman, *J. Am. Chem. Soc.* 80, 1339 (**1958**).
**41.** H. W. Kim, S. H. Shim, J. W. Lee, J. Y. Park, and S. S. Kim, *Chem. Phys. Lett.* 456, 193 (**2008**).
**42.** S. W. Choi, J. Y. Park, and S. S. Kim, *Nanotechnology* 20, 465603 (**2009**).
**43.** J. Y. Park, S. W. Choi, J. W. Lee, C. Lee, and S. S. Kim, *J. Am. Ceram. Soc.* 92, 2551 (**2009**).
**44.** J. Y. Park, S. W. Choi, and S. S. Kim, *Nanoscale Res. Lett.* 5, 353 (**2010**).
**45.** H. W. Kim, S.-W. Choi, A. Katoch, and S. S. Kim, *Sens. Actuators B* 177, 654 (**2013**).
**46.** H. K. Jeong, Y. P. Lee, R. J. W. E. Lahaye, M. H. Park, K. H. An, I. J. Kim, C. W. Yang, C. Y. Park, R. S. Ruoff, and Y. H. Lee, *J. Am. Chem. Soc.* 130, 1362 (**2008**).
**47.** K. N. Kudin, B. Ozbas, H. C. Schniepp, R. K. Prud'homme, I. A. Aksay, and R. Car, *Nano Lett.* 8, 36 (**2008**).
**48.** P. Gupta, T. Dutta, S. Mal, and J. Narayan, *J. Appl. Phys.* 111, 103706 (**2012**).
**49.** M. A. van Veenendaal and G. A. Sawatzky, *Phys. Rev. Lett.* 70, 2459 (**1993**).
**50.** M. Tyagi and M. Tomar, *IEEE Electron Dev. Lett.* 34, 81 (**2013**).
**51.** S. Deng, V. Tjoa, H.M. Fan, H.R. Tan, D.C. Sayle, M. Olivo, S. Mhaisalkar, J. Wei, and C.H. Sow, *J. Am. Chem. Soc.* 134, 4905 (**2012**).
**52.** J. D. Fowler, M. J. Allen, V. C. Tung, Y. Yang, R. B. Kaner, and B. H. Weiller, *ACS Nano* 3, 301 (**2009**).
**53.** D. Adler and J. Feinleib, *Phys. Rev. B* 2, 3112 (**1970**).
**54.** A. B. Kunz, *J. Phys. C* 14L, 445 (**1981**).
**55.** H. Sato, T. Minami, S. Takata, and T. Yamada, *Thin Solid Films* 236, 27 (**1993**).
**56.** H. J. Jang, C. J. Park, and H. S. Kwon, *Electrochim. Act.* 50, 3503 (**2005**).
**57.** D. R. Kauffman and A. Star, *Nano Lett.* 7, 1863 (**2007**).
**58.** D. R. Kauffman, D. C. Sorescu, D. P. Schofield, B. L. Allen, and K. D. Jordan, *Nano Lett.* 10, 958 (**2010**).




Received: 14 November 2014. Accepted: 27 January 2015.